Supporting Information

Disclose the origin of transition metal oxides as peroxidase (and catalase) mimetics

Bo Yuan[1], Hung-Lung Chou[2], Yung-Kang Peng[1,3]*

[1]Department of Chemistry, City University of Hong Kong, Hong Kong 0000, Hong Kong SAR.

[2]Graduate Institute of Applied Science and Technology, National Taiwan University of Science and Technology, Taipei 10617, Taiwan.

[3]City University of Hong Kong Shenzhen Research Institute, Shenzhen 518057, China.

*Email: ykpeng@cityu.edu.hk

Chemicals.

Sodium hydroxide (reagent grade, Sigma-Aldrich); sodium acetate (Sigma-Aldrich); acetic acid (AcOH, Sigma-Aldrich); ethanol (absolute ≥ 99.8% (GC), Sigma-Aldrich); hydrogen peroxide solution (30% (w/w) in H_2O, Sigma Aldrich); 3,3',5,5'-tetramethylbenzidine (TMB, Aladdin); 2,2'-azino-bis(3-ethylbenzothiazoline-6-sulfonic acid) (ABTS, Sigma-Aldrich); o-phenylenediamine (OPD, J&K); dopamine hydrochloride (Sigma-Aldrich); methyl blue (Macklin); rhodamine B (Macklin); phenol red (Aladdin); terephthalic acid (TA, Energy Chemical); 5,5-Dimethyl-1-pyrroline N-oxide (DMPO, >97%, Sigma-Aldrich). Common transition metal oxide nanoparticles (NPs) with averaged size < 100 nm were purchased mainly from Sigma-Aldrich and Aladdin. TiO_2 NPs (Sigma-Aldrich, P25); γ-Fe_2O_3 NPs (Aladdin); Fe_3O_4 NPs (Sigma-Aldrich); Co_3O_4 NPs (Aladdin); NiO NPs (Aladdin); Cu_2O NPs (Solarbio); CuO NPs (Aladdin); ZnO NPs (Sigma-Aldrich); CeO_2 NPs (Sigma-Aldrich).

Peroxidase-like activity and Michaelis-Menten kinetic study.

The peroxidase-like activity of commercial transition metal oxide NPs was investigated according to procedures below. To initiate the reaction, 15 μg NPs was dispersed in an as-prepared 1.5 mL buffer solution (NaAc-HAc acetate buffer, pH=4) containing 0.1 M H_2O_2 and 1 mM TMB (i.e., dye). The mixed solution was allowed to react for 7 min before the removal of NPs by centrifugation for another 3 min at 12,000 rpm. The amount of oxidized TMB in each supernatant was recorded by UV-Vis spectroscopy. To compare the activity of Fe_3O_4, CuO and Cu_2O NPs under similar surface area, the amount of Cu_2O was fixed at 15 μg and the amount for Fe_3O_4 and CuO can be calculated as 5.45 μg and 43.6 μg according to their surface area. The oxygen generated during this reaction was monitored using a dissolved oxygen meter (Leici, Shanghai, China). In addition to TMB, other dye substrates such as ABTS , OPD and dopamine often used for bioanalytical applications were also tested using the same concentration (i.e., 1 mM). Their oxidized products, $ABTS^{+\cdot}$ (from ABTS), diaminophenazine (from OPD) and aminochrome (from DA) can also be monitored at 418 nm, 448 nm and 480 nm by UV-vis spectroscopy. For Michaelis-Menten kinetic analysis, different concentration of H_2O_2 (0.5 mM-80 mM) were adopted to evaluate its affinity to Cu_2O and Fe_3O_4. The concentration of TMB was kept at 1 mM in the solution. The kinetic parameters were calculated according to the Michaelis-Menten equation:

$$v = V_{max} \frac{[S]}{([S] + K_m)}$$

where v is the reaction velocity, V_{max} is the maximal reaction velocity, [S] is the concentration of H_2O_2 and K_m is the Michaelis constant.

EPR detection of OH and HO₂ radicals.

EPR measurements were carried out in ambient on Bruker A300 with an X-band resonant cavity of 9.85 GHz. For the detection of OH radicals, 15 μg NPs was dispersed in an as-prepared 1.5 mL buffer solution (pH=4) containing 30 mM H_2O_2 and 50 mM DMPO and allowed to react for 1 min. NPs were removed by fitration and the supernatant was measured. For the detection of HO_2 radicals, methanol was used as the solvent with other conditions kept the same.

Fluorescent detection of OH radical.

To confirm the OH radical pathway, TMB used in procedures above was replaced by terephthalic acid (TA, 1 mM) which can form fluorescent 2-hydroxyterephthalic acid (TAOH) at 430 nm with OH radical. Similarly, 15 µg NPs was dispersed in an as-prepared 1.5 mL buffer solution (pH=4) containing 30 mM H_2O_2 and 1 mM TA and allowed to react for 7 min. NPs were removed by centrifugation for 3 min at 12,000 rpm and the supernatant was measured by fluorescence spectroscopy (Fluormax-4).

Dye degradation by Fenton process.

The Fenton-like activities of Cu_2O and Fe_3O_4 were examined using three conventional dyes such as rhodamine B, methyl blue and phenol red with characteristic absorption peak at 553 nm, 664 nm and 432 nm. For this reaction, 10 mg NPs were dispersed into 20 mL of dye solution (7.5 µg/mL) containing 0.5 M H_2O_2. The reaction was conducted at room temperature and 1 mL of solution was sampled at a given time point for analysis. The corresponding supernatant solution after centrifugation was recorded by UV-Vis spectroscopy (A_0: the initial absorption of dye in solution at its characteristic wavelength; A: the corresponding absorption at a given time point).

Catalase-like activity.

The evaluation of catalase-like activity was conducted by dispersing 15 µg samples in 1.5 mL of a freshly prepared H_2O_2 (5 mM) aqueous solution at 25 °C for 30 mins. The decomposition of H_2O_2 was monitored at 240 nm by UV-Vis spectroscopy (the molar extinction coefficient of H_2O_2 at this wavelength is 39.4 M^{-1} cm^{-1}) while the amount of O_2 produced was recorded by a dissolved oxygen meter.

Glutathione detection.

For glutathione detection, 15 µg NPs was dispersed in 1.5 mL acetate buffer solution (pH=4) containing 0.1 M H_2O_2 and 1 mM TMB. The mixed solution was allowed to react for 7 min before the removal of NPs by centrifugation for another 3 min at 12,000 rpm. The absorbance at 652 nm of this solution was recorded and denoted as A_0. Then, 0.15 mL of freshly prepared GSH solutions (0.01, 0.03, 0.05, 0.1, 0.3, 0.5, 1, 3, 5 mM) was then mixed with the solution above (final GSH concentration 1, 3, 5, 10, 30, 50, 100, 300, 500 µM) and allow to react for 10 min. The absorbance at 652 nm was recorded again and denoted as A. Then the changes in absorbance at 652 nm (i.e., A-A_0) can be plotted as a function of GSH concentration. And the limit of detection (LOD) for GSH was calculated according to LOD = 3(SD/B),where SD is the standard deviation of seven blank signals and B is the slope of the calibration curve[1]. For the selectivity test, solution B containing agarose, sucrose, cholesterol, glucose, D-sorbitol, sodium chloride and potassium chloride (5 mM) were further tested.

Computational detail.

The projector-augmented waves (PAW) [2-3] generalized gradient approximation (GGA) [4] was employed for density functional theory (DFT) simulation in this study. In the plane wave calculations, cutoff energy of 500 eV was applied, which was automatically set by the total energy convergence calculation for O-terminated Cu_2O (100), Cu-terminated Cu_2O (100) and Fe_3O_4(111) slab systems. Those surfaces were constructed as a slab within the three-dimensional periodic boundary conditions and a 14 Å vacuum layer was adopted perpendicularly to the surface. During the simulation for three slab systems, the bottom five layers were kept fixed to the bulk coordinates and full atomic

relaxations were allowed for the top five layers. A 3×3×1 k-Point mesh was used in the super cell. The unit cell size of the Fe_3O_4 (111) slab systems (6.033×6.033×23.237 Å^3) with the stable structure was adopted to perform the calculation of H_2O and H_2O_2 adsorption. For O-terminated and Cu-terminated Cu_2O(100) slab systems, the corresponding calculation was conducted in the cell dimension of 12.808 ×12.808×24.674 Å^3. The atoms in the cell were allowed to relax until the forces on unconstrained atoms are less than 0.02 eV/Å. Taking the adsorption of H_2O as an example, the adsorption energy (E_{ad}) is defined as the sum of interactions between H_2O and Fe_3O_4 (111) slab system, and it is given as $E_{ads} = E_{total} - E_{Fe3O4(111)} - E_{H2O}$, where E_{total}, $E_{Fe3O4(111)}$ and E_{H2O} are the total energy of the system, the energy of Fe_3O_4(111) slab system and H_2O molecule, respectively. The negative sign of E_{ads} corresponds to the energy gain of the system due to molecular adsorption. **Table S1** summarizes the calculated E_{ad} of H_2O and H_2O_2 on Fe_3O_4 (111), O/Cu-terminated Cu_2O (100) surfaces.
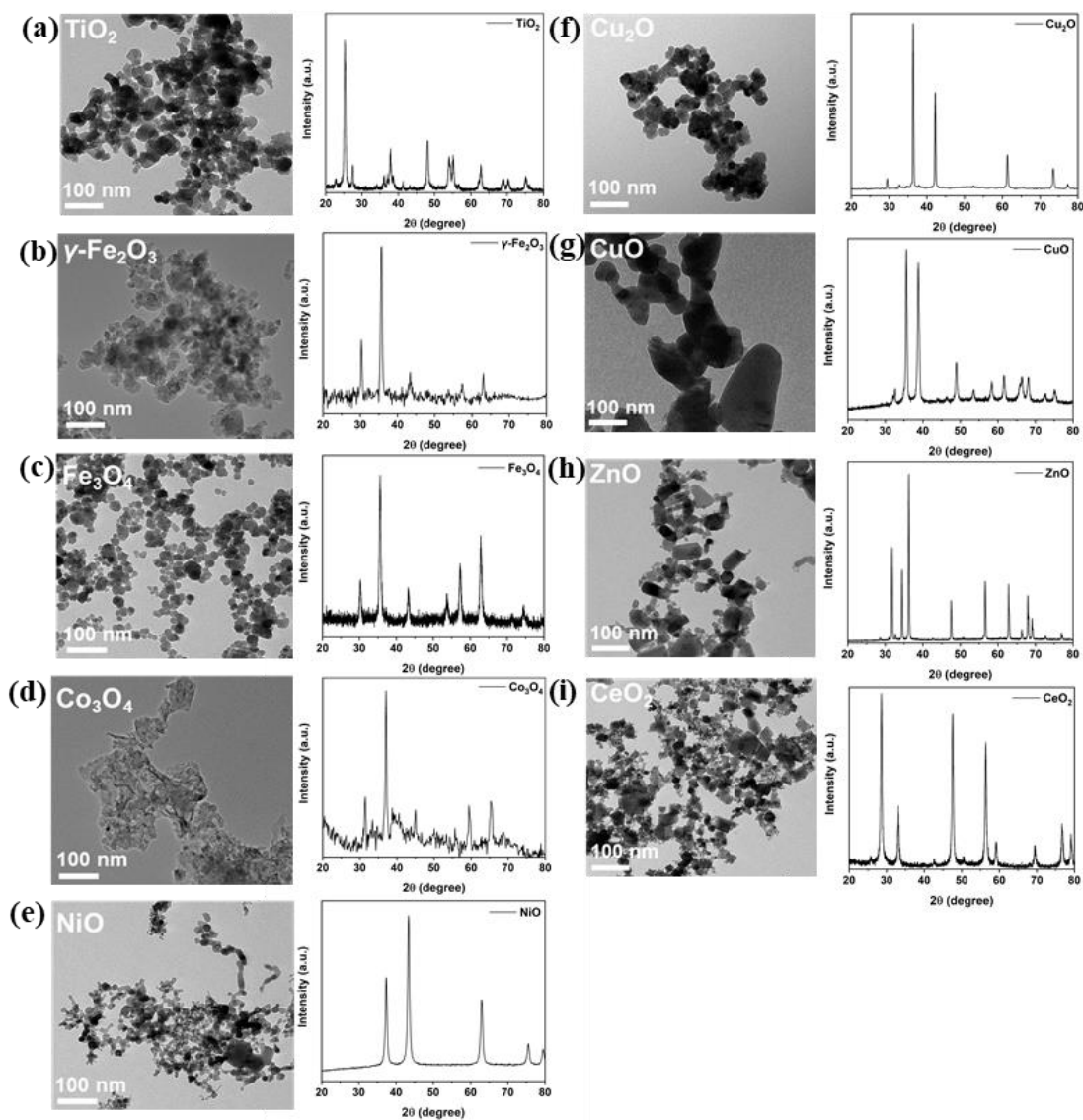
Figure S1. Transmission electron microscopy (TEM) images and X-ray diffraction (XRD) patterns of transition metal oxides (a) TiO_2, (b) γ-Fe_2O_3, (c) Fe_3O_4, (d) Co_3O_4, (e) NiO, (f) Cu_2O, (g) CuO, (h) ZnO and (i) CeO_2. See Figure S2 and Figure S3 for the detailed characterization of Fe_3O_4 and Cu_2O.
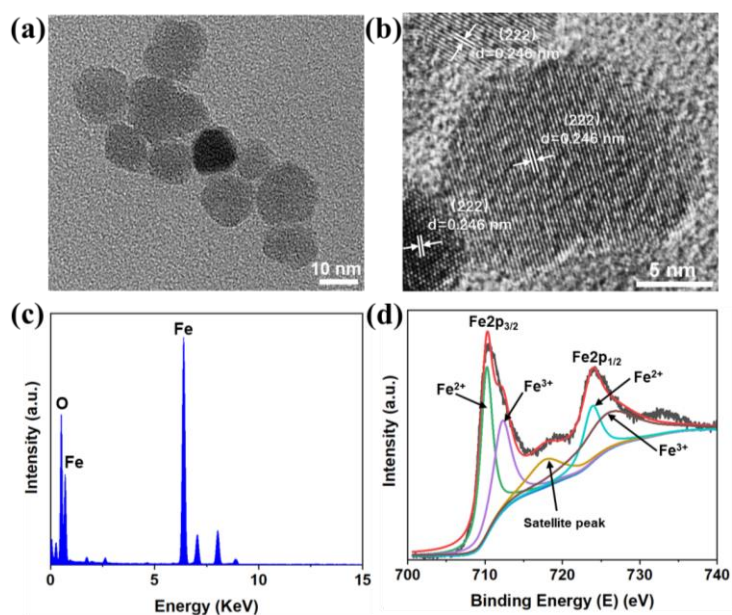
Figure S2. TEM images of Fe_3O_4 with (a) higher resolution and (b) lattice spacing. The corresponding elemental analysis by (c) energy-dispersive X-ray spectroscopy (EDS) spectroscopy and (d) X-ray photoelectron spectroscopy (XPS).
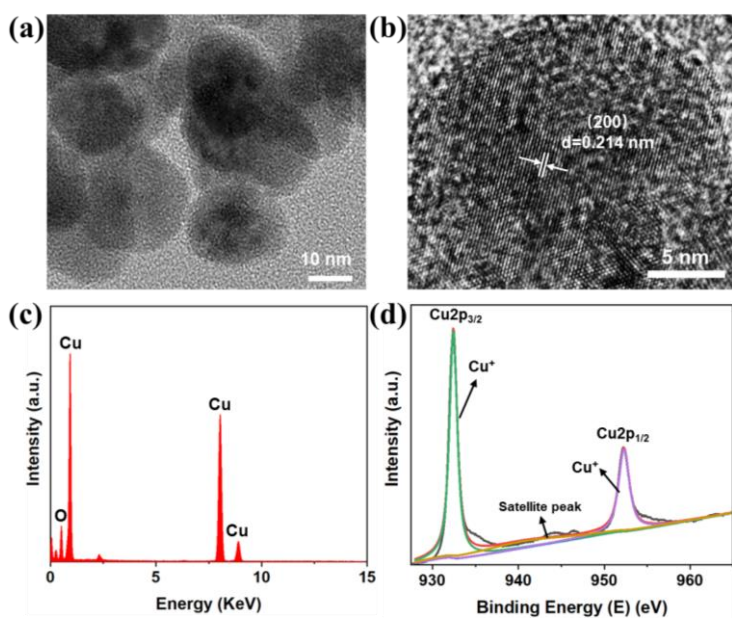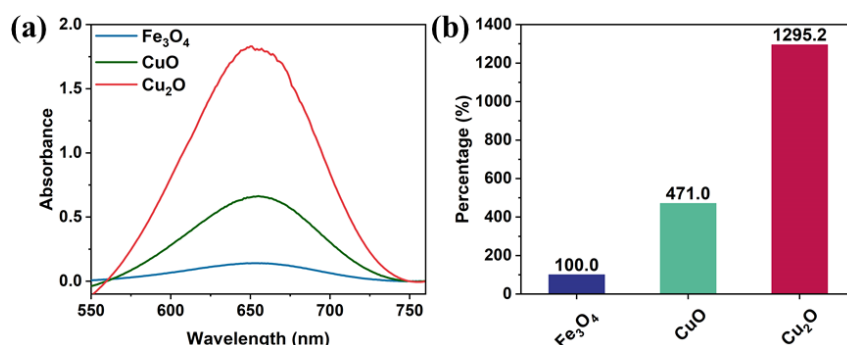

Figure S3. TEM images of Cu_2O with (a) higher resolution and (b) lattice spacing. The corresponding elemental analysis by (c) EDS and (d) XPS.
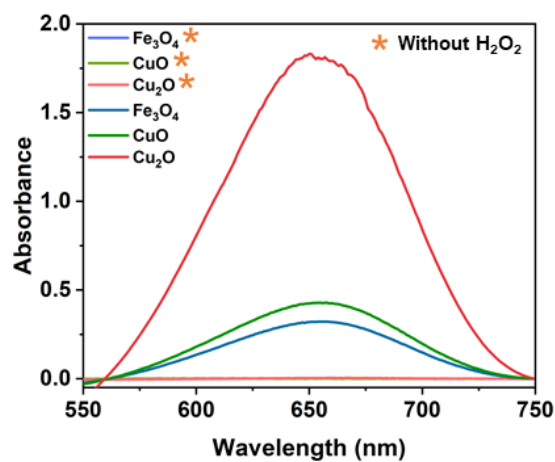
Figure S4. UV-vis spectra of Fe_3O_4, CuO, Cu_2O and the comparison of their activity w/o H_2O_2 (the same tested weight).
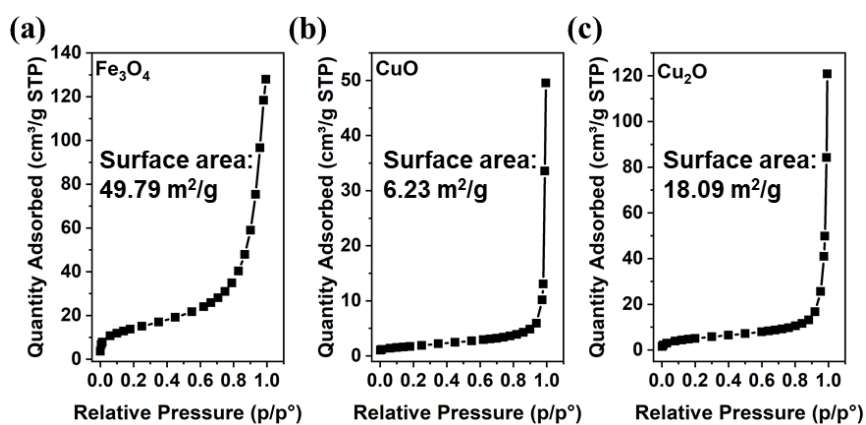
Figure S5. The N_2 adsorption/desorption isotherms and the Brunauer–Emmett–Teller (BET) surface area of (a) Fe_3O_4, (b) CuO and (c) Cu_2O.

Figure S6. (a) The UV-vis spectra and (b) the relative absorbance intensity of TMB_{ox} (652 nm) over Fe_3O_4, CuO, Cu_2O NPs with the same surface area for testing (i.e., 5.45 µg for Fe_3O_4, 43.6 µg for CuO and 15 µg for Cu_2O).
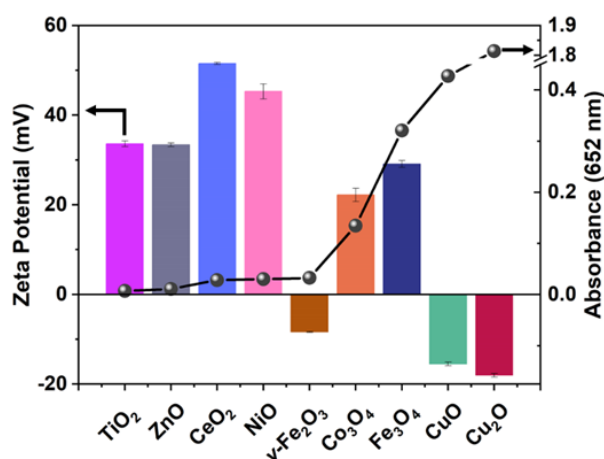

Figure S7. The zeta-potentials of commercial transition metal oxides used in this study and their comparison with corresponding peroxidase-like activity.

Since surface charge may affect the adsorption of H_2O_2 or TMB, we further compared their zeta-potentials with peroxidase-like activity (from the absorbance of TMB_{ox} at 652 nm). Despite the most active two oxides, Cu(II)O and Cu_2(I)O, both exhibit negative surface charge, the tiny difference between their charge cannot explain the high activity provided by Cu_2O. We believe this is mainly due to the difference in the redox velocity of H_2O_2 over $M^{(n+1)+}$ and M^{n+} as discussed in the manuscript. This can further be evidenced by γ-Fe_2O_3 with also a negative surface charge while gives a comparable activity to NiO and CeO_2 with very positive surface charge up to + 50 meV. It is thus concluded that the surface charge of a given nanozyme is not the key factor determining its peroxidase-like activity.
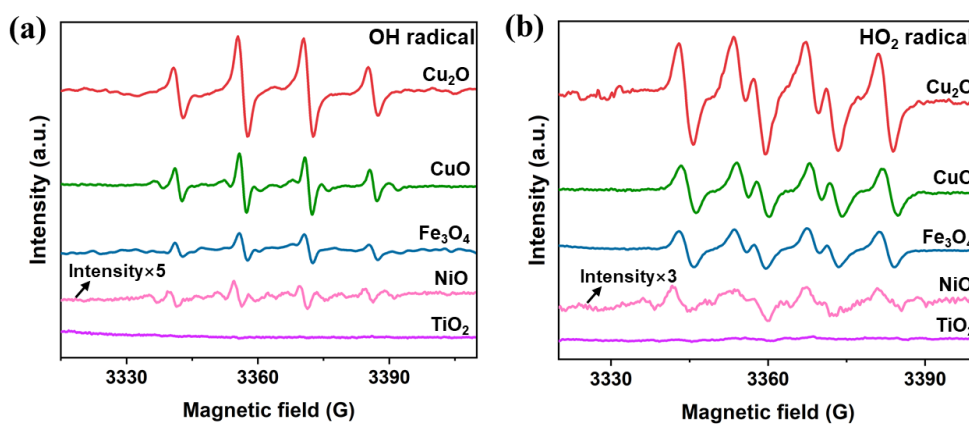
Figure S8. DMPO-assisted EPR monitoring the generation of (a) OH and (b) HO_2 radicals over Cu_2O, CuO, Fe_3O_4, NiO, and TiO_2 in the presence of H_2O_2.
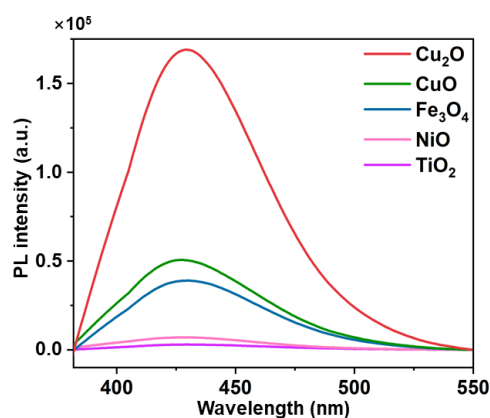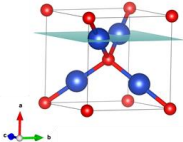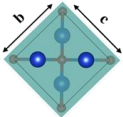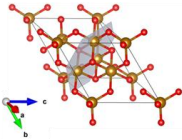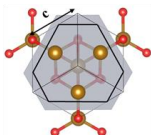

Figure S9. Using terephthalic acid (TA) as a fluorescent probe for the generation of OH radicals (from added H_2O_2) over Cu_2O, CuO, Fe_3O_4, NiO, and TiO_2. The order of peak intensity matches very well with the amount of OH radicals produced in Figure S8a.
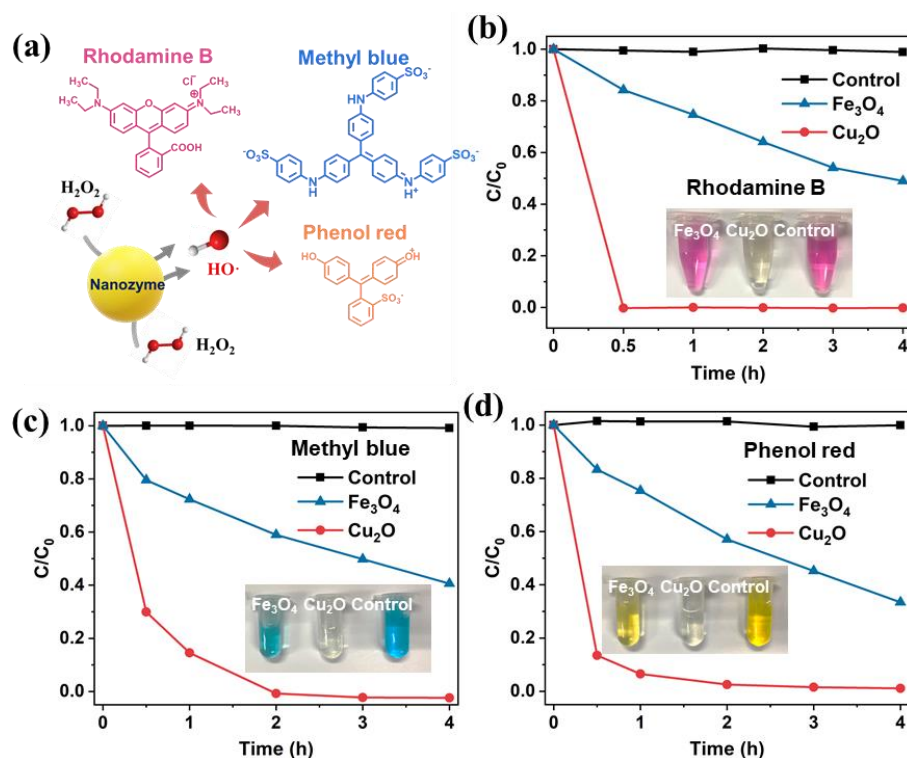
Figure S10. (a) Schematic illustration of the degradation of rhodamine B, methyl blue, phenol red over nanozyme with H_2O_2 and (b-d) their time-dependent degradation over Fe_3O_4 and Cu_2O. C_0 is the initial concentration of dye for reaction, C is the concentration of unreacted dye at a given time point.
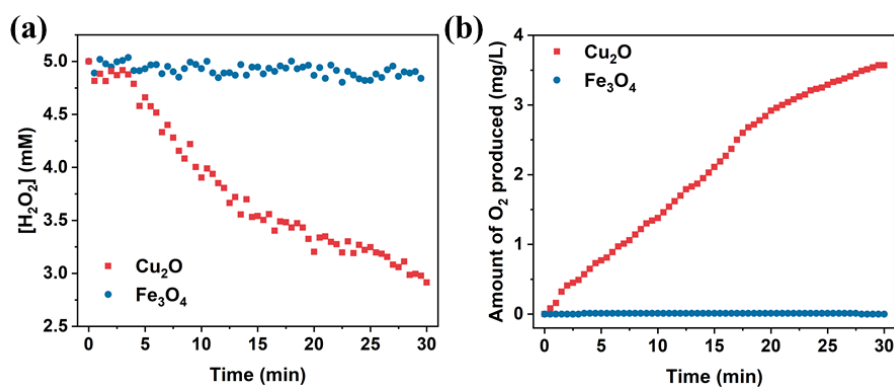
Figure S11. The catalase-like activity of Fe_3O_4 and Cu_2O. The evaluation of (a) H_2O_2 decomposition and (b) O_2 generation as a function of time.

|	Primitive cell	Facet	$= \dfrac{\text{area of slicing plane}}{\text{number of metal sites contained}}$ Area per active site (nm²)	Active sites per nm²
Cu_2O Lattice constant: a=b=c=4.288 Å $\alpha=\beta=\gamma=90°$		Cu-terminated $Cu_2O(100)$	$\dfrac{b \times c}{2} = 0.0919$	10.88
Fe_3O_4 Lattice constant: a=b=c=6.034 Å $\alpha=\beta=\gamma=60°$		Fe_{oct}-$Fe_3O_4(111)$	$\dfrac{\frac{\sqrt{3}}{4}(c^2+0.4662 \times c^2)}{3} = 0.0771$	12.97

Figure S12. The calculation of number of surface Cu and Fe sites on Cu-Cu₂O(100) and Fe₃O₄(111). The total number of active sites of a given crystallite can be obtained by knowing its surface area and the density of active sites on each facet. Note that Cu-terminated Cu₂O(100) was adopted for TOF calculation in this study due to the negligible adsorption energy of H₂O₂ on O-terminated Cu₂O (Figure 4e).
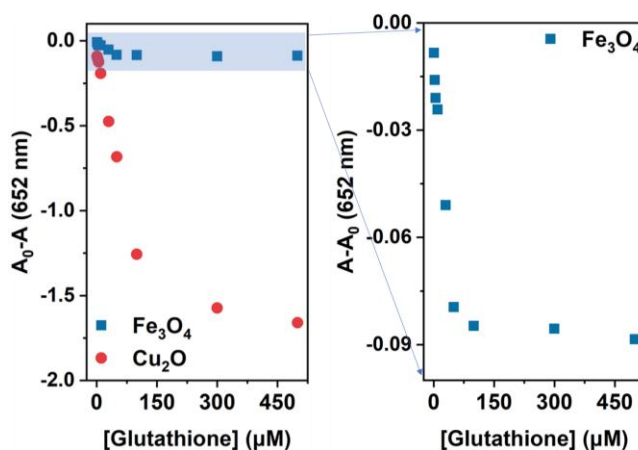
Figure S13. The enlarged Figure 6c for Fe₃O₄.
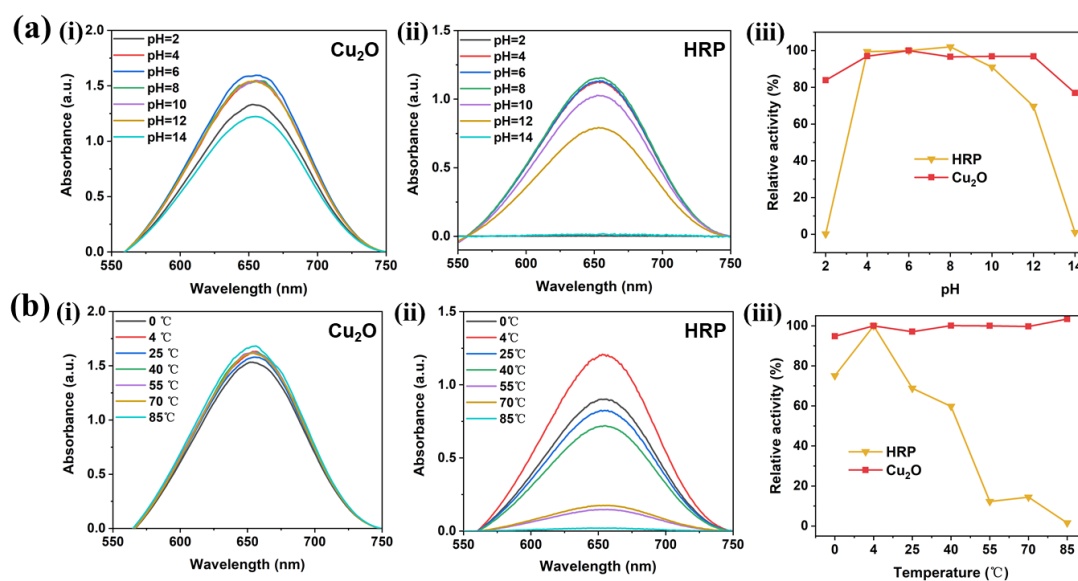
Figure S14. Comparison of (a) pH and (b) temperature stability of Cu$_2$O NPs and HRP. Both samples were pretreated at different pH (from 2 to 14) and temperatures (from 0 to 85 °C) for 3 hours before test. The UV-Vis spectra for (i) Cu$_2$O NPs and (ii) HRP. (iii) Further comparison by normalizing their activity obtained at pH = 6 or temperature at 4 °C (i.e., set as 100 %).

Table S1. The absorbance of TMB$_{ox}$ at 652 nm over transition metal oxides w/o H$_2$O$_2$. Note that the absorbance of Fe$_3$O$_4$ (with H$_2$O$_2$) was set as 100% for the calculation of percentage in both columns.

Catalyst	With H$_2$O$_2$		Without H$_2$O$_2$	
	Absorbance (652 nm)/a.u.	Percentage/%	Absorbance (652 nm)/a.u.	Percentage/%
TiO$_2$	0.007	2.3	0.0009	0.3
Fe$_3$O$_4$	0.321	100.0	0.0012	0.4
NiO	0.030	9.4	0.0015	0.5
Cu$_2$O	1.814	565.5	0.0016	0.5
CuO	0.427	133.2	0.0009	0.3

Table S2. Calculated adsorption energy (E$_{ad}$) of H$_2$O and H$_2$O$_2$ on Fe$_3$O$_4$(111), Cu-/O-terminated Cu$_2$O(100) surfaces. The calculated E$_{ad}$ of H$_2$O on Fe$_3$O$_4$(111) and Cu-Cu$_2$O(100) surfaces matches literature results very well[4, 5]. Note that the E$_{ad}$ of H$_2$O$_2$ on O-Cu$_2$O was too small to be converged.

System	Adsorbate	E$_{ad}$ (eV)	
		This work	Ref.
Fe$_3$O$_4$(111)	H$_2$O	-1.54	-1.45[4]
	H$_2$O$_2$	-1.32	/
Cu-Cu$_2$O(100)	H$_2$O	-0.71	-0.77[5]
	H$_2$O$_2$	-0.79	/
O-Cu$_2$O(100)	H$_2$O	-0.01	/

Table S3: Details of glutathione detection using Cu$_2$O and Fe$_3$O$_4$ as peroxidase mimetics.

Sample	LOD (µM)[a]	Linear range (µM)	Slope(10^{-3})	SD (10^{-3})[b]	R-square
Cu$_2$O	0.16	1-100	11.9	6.51	0.99
Fe$_3$O$_4$	1.48	5-50	1.44	7.09	0.99

[a]LOD: limit of detection. [b]SD: standard deviation.

References

(1) Dong, Z. Z.; Lu, L.; Ko, C. N.; Yang, C.; Li, S.; Lee, M. Y.; Leung, C. H.; Ma, D. L. A MnO_2 Nanosheet-Assisted GSH Detection Platform Using an Iridium(iii) Complex as a Switch-on Luminescent Probe. *Nanoscale* **2017,** *9* (14), 4677-4682.
(2) Vanderbilt, D. Soft Self-Consistent Pseudopotentials in a Generalized Eigenvalue Formalism. *Phys. Rev. B* **1990,** *41* (11), 7892-7895.
(3) Payne, M. C.; Teter, M. P.; Allan, D. C.; Arias, T. A.; Joannopoulos, J. D. Iterative Minimization Techniques for ab Initio Total-Energy Calculations: Molecular Dynamics and Conjugate Gradients. *Rev. Mod. Phys.* **1992,** *64* (4), 1045-1097.
(4) Perdew, J. P.; Chevary, J. A.; Vosko, S. H.; Jackson, K. A.; Pederson, M. R.; Singh, D. J.; Fiolhais, C. Atoms, Molecules, Solids, and Surfaces: Applications of the Generalized Gradient Approximation for Exchange and Correlation. *Phys Rev B Condens Matter* **1992,** *46* (11), 6671-6687.